Amino grafted MCM-41 as highly efficient and reversible ecofriendly adsorbent material for the Direct Blue removal from wastewater

Vito Rizzi[a], Eko Adi Prasetyanto[b], Pengkun Chen[b], Jennifer Gubitosa[a], Paola Fini[c], Angela Agostiano[a,c], Luisa De Cola[b*] and Pinalysa Cosma[a,c*]

[a]Università degli Studi "Aldo Moro" di Bari, Dip. Chimica, Via Orabona, 4- 70126 Bari, Italy

[b]ISIS & icFRC, Université de Strasbourg & CNRS, 8 rue Gaspard Monge, 67000 Strasbourg, France

[c]Consiglio Nazionale delle Ricerche CNR-IPCF, UOS Bari, Via Orabona, 4- 70126 Bari, Italy.

ABSTRACT

The very high adsorption efficiency of Direct Blue (DB), an anionic toxic azo dye, onto amino grafted mesoporous silica nanoparticles (MCM-41), was studied in this paper, for possible industrial applications. Interesting challenges and advances are proposed in this field, presenting an adsorbent able to efficiently and rapidly remove the anionic dye from water. The important added value of this work regards the system recycle, which allows both the DB and adsorbent material recover, with a global reduction of the environmental impact, in the viewpoint of the green economy. Indeed, this paper is the first example of very fast removal and recycle of great amounts of DB with adsorbent materials characterized by impressive adsorption/desorption capacities, at least of around 300 mg/g for each adsorption cycle, potentially increasable by performing

1

1   consecutive cycles of DB adsorption/desorption. In detail, the MCM-41 amino functionalization

2   (MCM-41-NH$_2$) was obtained after (MCM-41-POST) and during (MCM-41-PRE) the synthesis

3   of MCM-41, obtaining materials with different behavior towards the DB adsorption. The MCM-

4   41-NH$_2$ surface features and porous structure, before and after the dye adsorption, were carefully

5   characterized. Considering the adsorption process, for investigating the nature of the DB/MCM-

6   41-NH$_2$ interaction, several parameters were studied: the contact time, the DB solutions pH values,

7   adsorbent material and dye amount, with the additional analysis of how the adsorption process was

8   influenced by the presence of electrolytes. The isotherms of adsorption were also considered.

9   Although MCM-41-PRE exhibited a higher affinity towards DB molecules, the MCM-41-POST

10   were able to rapidly desorb it, thus recycling both DB and the adsorbent material.

11

12   **KEYWORDS**: Wastewater; Adsorption; Silica; Mesoporous materials; Direct dyes; MCM-41.

13

14   **1. INTRODUCTION**

15   Since several years, the problem related to the introduction of pollutants in the environment is

16   highlighted as a worldwide alarm. The nature of these wastes is ranging from inorganic to organic

17   products usually used in several application fields.[1] Among pollutants, dyes represent an

18   important class of dangerous compounds, since the discharge of dye-bearing wastewater into

19   natural streams and rivers from textile, paper, carpet, leather, distillery, and printing industries

20   affects both the life of aquatic organisms and human health.[2] Indeed, the dangerous by-products

21   formation, from oxidation, hydrolysis, or other chemical reactions in the wastewater, is one of the

22   major problems occurring when dyes are discharged in water.[3] Since textile industries employ

23   large volumes of water and chemicals for textile wet-processing, they are rated as the most

1   pollutant among all industrial sectors, draining more than 5000 tons of dyes every year.[4] The

2   dye chemical classes more frequently employed on industrial scale are anthraquinone-, sulfur-,

3   indigoid-, triphenylmethyl (trityl), phthalocyanine- and azo-derivatives, however, the latter are

4   considered as the most common.[5] As reported by Rizzi *et al.*[6], notwithstanding the release of

5   these dyes into environment is of great concern, due to both their highly visible color in water, and

6   their toxicity, mutagenicity and carcinogenicity, dyes still continue to find new applications in

7   various high-technology areas.[6] Therefore, the dye removal from wastewater is a growing area

8   of research, with the challenge to develop highly and cheap performant technologies to treat

9   wastewaters.[7-15] For this purpose, different methods have been proposed and among them the

10   physical adsorption is one of the most effective methods for removing color from water.[15,16]

11   Seow *et al.*[17] emphasized that the adsorption process is usually preferred for wastewater

12   treatments, with activated carbon as one of the most used commercial adsorbent material for these

13   purposes.[17] However, due to the high cost of production and low levels of regeneration of such

14   a material, the market is trying to replace this adsorbent.[18-23] Additionally, the possibility to

15   reuse both dyes and adsorbent materials is another important challenge of research related to the

16   possibility of recycling dyes and adsorbent, in the viewpoint of a circular eco-sustainable economy

17   (material recycling and product re-use).[6]

18   Sorbents based on mesoporous silica have attained considerable attention due to their highly

19   ordered structure, nanometer-sized pores, and their high surface area.[24-26] More specifically,

20   the ordered porous structure induces a much easier diffusion of several target molecules into the

21   active sites, compared with the most part of the adsorbent materials.[18-26] For example, MCM-

22   41 hybrid materials were studied for the adsorption of Acid Red G with adsorption capacities (q_{max})

23   of around 100 mg/g.[27] An adsorbent MCM-41-based was selected for the removal of Alizarin

1   Yellow with q_{max} of 121.95 mg/g.[28] Qin *et al.* [29] indicated the efficient removal of dyes using

2   mesoporous silica nanoparticles, finding q_{max} values in the range 14.70 mg/g-34.23 mg/g. Other

3   typologies of mesoporous materials were used for this purpose and, among them, SBA-15 showed

4   interesting results. Mirzaie *et al.* [30] reported as the optimum conditions of work to remove dyes

5   required an very acid initial pH and long contact time. Nanocomposite polypyrrole/SBA-15 were

6   also described.[31] For these studies, the recorded adsorbed amounts for dyes were 41.66 and

7   58.82 mg/g, respectively. Dong *et al.*[32] showed also very interesting results indicating the

8   possibility to reuse the adsorbent. More specifically, nonetheless the q_{max} value was very high, 280

9   mg/g, the calcination to reuse the adsorbent for several adsorption cycles was proposed by

10 Authors.[32] Starting from these considerations, in the present paper amino grafted MCM-41 with

11 a mean size of 100 nm and channels of approximately 4 nm wide, were used for exploring their

12 capacity in the DB uptake from water. Indeed, the adsorption and desorption occurred in very short

13 time, and the materials showed high q_{max} values (10-300 mg/g for each adsorption cycle) if

14 compared with literature.[27-32] Furthermore, in the present paper, the anionic dye desorption and

15 the adsorbent recycle are presented as a pH dependent mechanism. Indeed, the use of alkaline

16 solutions enabled the recovery of the dye together with the adsorbents recycle, avoiding the use of

17 organic solvent, as ethanol[29] and/or hard disruptive conditions of work for dyes, as the adsorbent

18 calcination after the dyes adsorption.[32] In this way the maximum adsorption capacity should be

19 also increased by using the same adsorbent.

20 It is worth to mention that CTAB (cetyl trimethylammonium bromide) was used as template agent

21 to induce the porous array formation, while the amino grafting was obtained by using the APTES

22 ((3-Aminopropyl) triethoxysilane). The latter was added during and after the synthesis of MCM-

23 41, obtaining two types of amino grafted MCM-41 (MCM-41-PRE and POST synthesis,

1   respectively). It is noteworthy, that for MCM-41-POST, the CTAB was completely removed after

2   the synthesis by calcination at 550°C, and the APTES was soon after added for the grafting;

3   whereas, the functionalization performed during the synthesis (MCM-41-PRE) did not allow the

4   use of high temperatures, since amino groups were present already from the beginning of the

5   synthesis. In that case, notwithstanding the washing with ethanol, a slight amount of CTAB was

6   found to be entrapped inside the pores. The effects of various operating parameters, affecting the

7   DB adsorption process, including the adsorbent dose, initial concentration of the aqueous dye

8   solution, the solution pH and the electrolyte influence were carefully investigated. The kinetic

9   analysis was also applied for determining the adsorption mechanism. The UV-Visible absorption

10   spectroscopy, monitoring the dyes spectra in water, was used to infer information. Further, a

11   MCM-41 and MCM-41-NH_2 comprehensive investigation (before and after the DB adsorption)

12   was performed in our laboratory using several complementary techniques: Thermo-Gravimetric

13   Analysis (TGA), Scanning Electron Microscopy (SEM), Transmission Electron Microscopy

14   (TEM), Small angle X-ray diffraction (SAXS), nitrogen adsorption isotherms and Zeta-potential

15   investigation. The evaluation of DB lifetime (after the adsorption and release processes) was also

16   carried out for demonstrating the absence of DB degradative processes. Among the studied

17   materials, MCM-41-PRE exhibited a slightly greater affinity towards DB than MCM-41-POST,

18   showing a very fast and easy method for anionic dyes removal from water. More specifically, the

19   inexpensive MCM-41-POST was able to completely release the adsorbed dye, enabling several

20   adsorption/desorption cycles.

21   **2. EXPERIMENTAL SECTION**

22   **2.1. Chemicals.** All the used chemicals were of analytical grade and samples were prepared

23   using double distilled water. Direct Blue 78 (chemical formula: $C_{42}H_{25}N_7Na_4O_{13}S_4$, MW: 1055.1

1   g·mol^{-1}), received by Colorprint Fashion, was used without further purification in order to mimic

2   the real pollutant problem (**Scheme 1**).
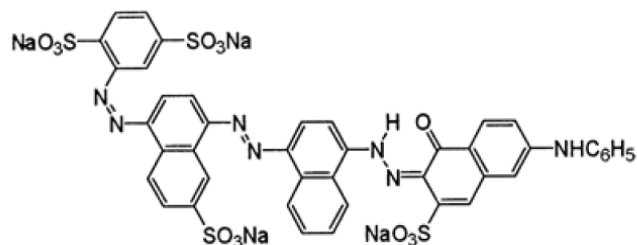
Scheme 1: DB 78 chemical structure.

3

4   Dye stock solution at a concentration of 1.0×10^{-4}M was prepared and dilutions were carried out

5   with double distilled water for obtaining the following dye concentrations, 5.0×10^{-5}M and

6   1.0×10^{-5}M. The pH values of various aqueous solutions were adjusted using concentrated HCl

7   (0.5M) and NaOH (1M) solutions. The following chemicals: NaH_2PO_4, TEOS (Tetraethyl

8   orthosilicate), APTES (3-Aminopropyl) triethoxysilane, CTAB (cetyl trimethylammonium

9   bromide), Ethanol, Methanol, Acetic acid, Ninhydrin, and anhydrous toluene were purchased from

10   Sigma-Aldrich.

11   **2.2. Synthesis of MCM-41-NH$_2$.** The procedure for the MCM-41-NH$_2$ synthesis is reported in

12   the following:

13   *Solution A:* 0.5 gram of CTAB and 1.75 mL of NaOH (2M) were mixed and dissolved in 240

14   mL of deionized water. The solution was stirred and heated at 80°C until the complete dissolution

15   of CTAB.

16   *Solution B*: 2.5 mL of TEOS were added into 3 mL of ethanol. In that solution, in order to obtain

17   only MCM-41-PRE, 100μL of APTES were added.

1   *Solution A* and *B* were mixed together stirring the solution at 80°C for 4h. A white precipitate

2   was obtained (as-synthesized MCM-41), then washed with methanol and dried overnight. The as-

3   synthesized MCM-41 powder were calcined at 550°C in air for 7h in order to remove the surfactant

4   from the pores. To obtain MCM-41-POST, 0.1 mL of APTES per gram of MCM-41 were added

5   after the calcination, stirring and refluxing the solution in dried toluene for 3h at 100°C. In the case

6   of MCM-41-PRE, surfactant molecules were removed with ethanol at 80°C under continuous

7   reflux for 24h.

8   **2.3. Determination of the MCM-41 amino grafting degree.** The degree of MCM-41 amino

9   grafting was inferred by the ninhydrin assay and TGA. In TGA, an appropriate amount of the

10   sample is heated at a specific heating rate and is monitored as a function of time or temperature.

11   The observed points of inflection in the TGA curves correspond to stages in which the weight loss

12   occurred.[25,26]

13   In this case, since the inorganic nature of the silica backbone, the weight losses can be certainly

14   attributed to the presence of amino groups. With regard the ninhydrin assay, the of Tung Lu's

15   procedure[25] was adopted for our systems. Ninhydrin reagent reacted with APTES at various

16   known concentrations forming colored products, arisen from the reaction with amino groups.

17   Afterward, the absorbance value of these samples at 570 nm was recorded to infer the calibration

18   curve, by plotting the absorbance value at 570 nm vs. the known amount of APTES. As a result,

19   the concentration of unknown samples can be inferred. More specifically, a weighted MCM-41-

20   POST/PRE amount, *W*, was added to a sodium acetate/acetic acid buffer solution (1 mL, 0.5M)

21   containing 2 mL of 0.2 % ninhydrin. Subsequently, that mixture was heated at 100°C for 15 min

22   and cooled at r.t. Finally, a dilution with 1 mL of an ethanol/water (1:1) solution was obtained. In

23   order to determine the absorption value at 570 nm, the mixture was centrifuged (Eppendorf

1   Minispin/Minispin Plus Microcentrifuges) analyzing the supernatant volume, designated as V (L),

2   by using a UV-Vis spectrophotometer. The molar quantity of amine (A, mol/g) grafted on MCM-

3   41 was evaluated in accordance with the following equation:

4    $$A\left(\frac{mol}{g}\right) = \frac{MV}{W}$$ **(1)**

5   M represents the molar concentration of amino groups determined by means of the calibration

6   curve.[18]

7   **2.4. Adsorption experiments.** The *in batch* equilibrium experiments were carried out for

8   exploring the adsorption behavior by adding appropriate and fixed powder amounts of adsorbent

9   materials (from 0.4 to 12.0 mg) into flasks containing 2 mL of dye solution at different initial dye

10   concentrations (5.0×10^{-5} M and 1.0×10^{-5} M, meaning 0.05 mg/1 mL and 0.01 mg/1 mL,

11   respectively). It is worth to mention the 0.4 mg of adsorbent was the lowest used dosage to be able

12   to significantly adsorb in short time the added dye amounts in water. The studied dye

13   concentrations were selected to mimic a high degree of DB dye pollution in water as suggested by

14   Colorprint Fashion. The flasks were sonicated in a water-bath for 5 minutes and then stirred

15   constantly until the complete adsorption of dye from water. Aqueous dye solutions were separated

16   from MCM-41/MCM-NH$_2$ powder by centrifugation at 14.5 rpm for 10 minutes. The dye

17   concentration was thus evaluated using a double beam UV/Vis spectrophotometer by measuring

18   the DB absorbance intensity at λ=600 nm at each adopted contact time. Moreover, experiments

19   were performed changing several parameters such as the pH of dye aqueous solutions, from 2 to

20   12 units, and evaluating at neutral pH the effect of an electrolyte. In that case, phosphate buffer

21   solutions at concentrations ranging from 1.0×10^{-4} M to 2.0×10^{-1} M were adopted in order to

22   maintain constant the pH value of dye solutions (pH 7).

1   In accordance with several studies reported in literature [6,11] and related to the dye adsorption

2   from wastewater, the adsorption capacity q_t (mg×g^{-1}) at time t of DB, was evaluated by applying

3   the following equation:

4

5    $$q_t = \frac{C_0 - C_t}{W} \times V \qquad\qquad (2)$$

6

7   where V represents the used total volume of solution (herein 2 mL), W is the weight of the dry

8   adsorbent material (g), C_0 and C_t represent the initial concentration and the concentration at time t

9   for the dye (mg×L^{-1}).

10   **2.5. Adsorption kinetics.** With the aim to study the experimental data trend, the pseudo first

11   and second–order kinetic models were adopted. More specifically, Equations 3 and 4 report the

12   linearized form of these models, respectively or else known as the Lagergren and Ho'

13   equations[33]:

14

15    $$\log(q_e - q_t) = \log(q_e) - \frac{K_1}{2.303} t \qquad\qquad (3)$$

16

17   q_e and q_t represent the adsorption capacities at equilibrium and at time t, respectively (mg×g^{-1})

18   and k_1 is the rate constant of the pseudo-first order adsorption (L×min^{-1}). [34]

19

20    $$\frac{t}{q_t} = \frac{1}{K_2 q_e^2} + \frac{1}{q_e} t \qquad\qquad (4)$$

21

9

1   q_e is the equilibrium adsorption capacity and k_2 ($g \times mg^{-1} min^{-1}$) the pseudo-second order

2   constant. The latter is easily determined from the slope and intercept of the plot t/q_t versus t. The

3   two models were employed, in this work, to describe the adsorption process of DB on MCM-41-

4   NH$_2$, searching and showing the best one describing the process.[2,6,11,35]

5   **2.6. Adsorption Isotherms.** The Langmuir, Freundlich and Temkin [11] isotherm equations

6   were used to study the removal of DB on MCM-41. Langmuir model describes the adsorption on

7   homogeneous surfaces with uniformly energetic adsorption sites and monolayer coverage.

8   **Equation 5** reports the adopted linear form:

9

10
$$\frac{C_e}{q_e} = \frac{1}{K_L \, Q_0} + \frac{C_e}{Q_0} \tag{5}$$

11

12   where q_e (mg$\times$g^{-1}) is the adsorbed amount of DB at equilibrium, C_e is the equilibrium concentration

13   of the DB (mg$\times$L^{-1}) in solution, K_L is Langmuir equilibrium constant (L$\times$mg^{-1}) and Q_0 the

14   maximum adsorption capacity (mg$\times$g^{-1}). When the Freundlich isotherm is applied, the assumption

15   of the model is that the surface of the adsorbent is heterogeneous and adsorption sites have different

16   energy of adsorption. The energy of adsorption changes as a function of the surface coverage.

17   **Equation 6** reports the linear form of this equation.

18

19
$$\log(q_e) = \log(K_F) + \frac{1}{n}\log(C_e) \tag{6}$$

20

21   where K_F (L$\times$mg^{-1}) is the Freundlich constant and n is the heterogeneity factor. K_F is related to the

22   adsorption capacity, whereas the 1/n value indicates if the isotherm is irreversible (1/n=0),

1   favorable ($0<1/n<1$) or unfavorable ($1/n>1$). The Temkin model in its linear form was also adopted

2   and the **Equation 7** was used.

3

4   $$q_e = B_1 \ln(K_T) + B_1 \ln(C_e) \tag{7}$$

5

6   The isotherm constants B_1 and K_T are inferred from the slope and the intercept of **Equation 7**,

7   respectively. K_T is the equilibrium binding constant ($L \times mol^{-1}$) corresponding to the maximum

8   binding energy and B_1 is related to the heat of adsorption. The model indicates that the heat of

9   adsorption linearly decreases during the adsorption process. The adsorption is characterized by a

10 uniform distribution of binding energies.

11

12   **2.7. Instrumental details.** Visible absorption spectra were recorded using a Shimadzu UV-Vis

13 spectrophotometer mod. 1601. Spectra were recorded in a 300–800 nm range, at a 1 nm/s scan rate

14 using a cuvette with a 1 cm path length. FTIR-ATR spectra were recorded within the 600–4000

15 cm^{-1} range using a Fourier Transform Infrared spectrometer 670-IR (Varian Inc., now Agilent

16 Technologies Inc., Santa Clara, CA, USA), whose resolution was set to 4 cm^{-1}. 32 scans were

17 summed for each acquisition. TGA were obtained using STA 449 F1 Jupiter, Netzsch apparatus

18 analyzing the samples in the range 25-550°C in air atmosphere. SAXS measurements of samples

19 were performed with SAXSess Small-angle X-Ray Scattering instrument (Anton Paar GmbH,

20 Austria). The Kratky type camera is attached to a laboratory X-Ray generator (PW3830, PAN

21 alytical), and was operated with a fine focus glass sealed X-Ray tube at 40 kV and 50 mA (Cu Kα,

22 α=0.1542 nm). Detection was performed with the 2D imaging plate and analyzed by an imaging

23 plate reader Cyclone® (Perkin Elmer). Measurements were performed with standard solid sample

1   holder for 30 min. The two-dimensional intensity data were converted to one-dimensional data

2   with SAXSQuant software (Anton Paar GmbH, Austria).

3   The adsorption–desorption isotherms of samples were measured at 77 Kusing N2 Micrometrics

4   ASAP 2020 Surface area and Porosity Analyzer to determine the average pore diameter. SEM

5   images were obtained using FEI Quanta FEG 250. Samples were placed on an aluminum stub and

6   metalized with gold. TEM images were obtained on a Philips CM120 transmission electron

7   microscope operating at 100 kV with a LaB6 filament. Areas covered with molecules of interest

8   were recorded under low dose condition, on a Pelletier cooled CCD camera (Model 794, Gatan,

9   Pleasanton, CA). The surface charge investigation of the MCM-41-NH2, at different pH values,

10   was also performed and searched through the Zeta potential measurements using a Delsa Nano C

11   Particle Analyzer (Beckman Coulter, Brea, CA, USA). Measurements were performed in

12   phosphate buffered saline (PBS), pH=7.4.

13

14   **3. RESULTS AND DISCUSSION**

15   As a preliminary step of this study, the MCM-41-NH2 used for the adsorption of DB were

16   carefully characterized by adopting several complementary techniques as reported in the

17   following.

18   **3.1 Microscopic investigation, N2 adsorption-desorption isotherms and SAXS analysis.** A

19   clear uniform distribution of spherical MCM-41-NH2, as well as the absence of aggregation of

20   those to macrospheres, are clearly observed during the SEM investigation. Indeed, as shown in the

21   image reported in **Figure 1A**, MCM-41-NH2 having a mean size of around 100 nm were obtained.

22   Additionally, as shown in **Figure 1B,** the highly ordered MCM-41-NH2 porous mesostructure was

23   evidenced by TEM analysis, highlighting the presence of ordered channels 4 nm wide.
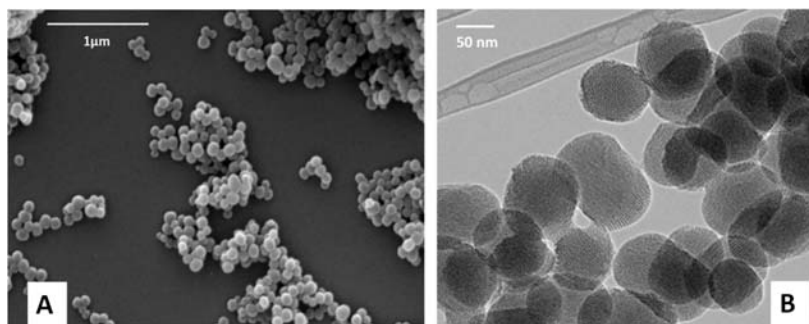
Figure 1: The SEM microphotograph (**A**) and TEM image (**B**) of MCM-41-NH$_2$.

1

2   To further investigate the pore size distribution of MCM-41-NH$_2$, the N$_2$ adsorption-desorption

3   isotherms were acquired and are reported in **Figure 2A**.

4   The obtained curves represented the typical reversible isotherms of mesoporous materials

5   usually indicated as Type IV isotherms.[36-38] More specifically, two steps are observed in

6   **Figure 2A**: the former between 0.10 and 0.25 *P/P$_0$*, due to the capillary condensation inside the

7   mesopore channels, followed by a slower growth in the adsorbed volume, and the latter up to *P/P$_0$*

8   = 0.9 due to an high N$_2$ adsorption/desorption volume. In excellent agreement with literature,[3]

9   such a behavior indicated the existence of MCM-41-NH$_2$ accessible mesoporous structure. The

10   sharpness of these steps also displays the uniform and narrow size distribution of mesopores.[3]

11   Accordingly, in **Figure 2B**, the experimental pores size distribution of MCM-41-NH$_2$ is reported

12   detecting the presence of one sharp peak centered at around 3.4 nm with a pore volume of 0.031

13   cm^3/g.

14   These findings well agree with SAXS measurements. Indeed, in **Figure 2C**, the SAXS pattern of

15   MCM-41-NH$_2$ is evidenced. The same was obtained for bare MCM-41. An intense diffraction

16   peak was observed having a q value of 1.5 nm^{-1}. A d-spacing value ($2\pi/q$), between the channels,

17   approximately of 4 nm was thus inferred.[39] Interestingly, according to literature [40], in which

1   other minor diffraction peaks are contemplated for MCM-41, at higher q values, minor signals

2   were observed (in our case slightly detected around a q value of 3 nm^{-1} as broad and slightly evident

3   signals); so this finding indicated some further reduction of the long-range order of the MCM-41

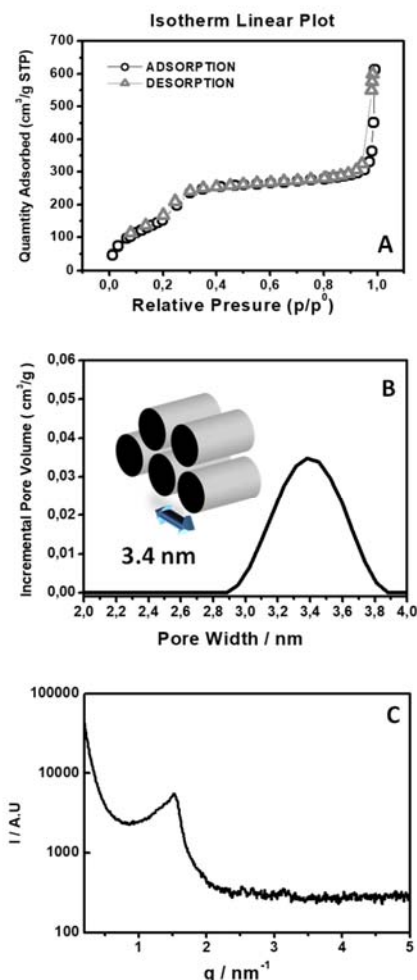4   framework, as observed in other studies related to grafted MCM-41 materials.[40]

Figure 2: Nitrogen adsorption Isotherms linear plot of the examined MCM-41-NH$_2$, function of the relative pressure p/p_0 (**A**); Pore size distribution of MCM-41-NH$_2$ (**B**); SAXS patterns of MCM-41-NH$_2$ (**C**).

5

6   **3.2 TG analysis and the ninhydrin assay.** In order to show differences before and after the

7   amino grafting, the TG curves of both MCM-41 and MCM-41-NH$_2$ were acquired and are shown

8   in **Figure S1A**. If the absence of mass losses was detected for MCM-41 (black solid line),

9   strengthening the absence of functional amino groups, conversely the presence of two main mass

1   losses in the TG curves, observed when MCM-41-NH$_2$ (MCM-41-POST, green line and MCM-

2   41-PRE, blue line) were taken into account, indicated the presence of the successfully amino

3   grafting. More specifically, the former mass loss, from about 25 to 140°C, was likely due to

4   physically adsorbed water on the surfaces of MCM-41-NH$_2$,[39] on the other hand the latter, from

5   140 to about 550°C, was ascribed to the introduced organic amino groups.[39] Interestingly, in the

6   second stage, the mass losses were different if MCM-41-POST and MCM-41-PRE are compared.

7   Regarding to this, it is worth to remember that, if the grafting POST synthesis was performed after

8   the calcination of MCM-41 at 550°C, with the total removal of the CTAB used as template agent,

9   conversely for MCM-41-PRE, the introduction of amino groups was obtained during the synthesis,

10   by removing the CTAB excess by washing in ethanol at 80°C. Therefore, the slight contribute of

11   CTAB molecules should be considered, evaluating the MCM-41-PRE mass losses. [41]

12   In order to quantitively estimate the amino grafting on the particles, the ninhydrin test was

13   performed.[39] A calibration curve using the APTES was preliminary obtained (**Figure S1B**) and

14   **Equation 1** was used to evaluate the molar amino grafting quantity (A, mol/g), based on the

15   weights of MCM-41-NH$_2$ (5.0 mg and 4.5 mg for MCM-41-POST and PRE, respectively). The

16   following values were obtained: 0.008 mol/g and 0.009 mol/g for MCM-41-PRE and POST,

17   respectively. So, even though the TGA results, while confirming the certain introduction of amino

18   groups on MCM-41-NH$_2$, indicated some differences in the amino groups distribution between

19   MCM-41-PRE and POST, the ninhydrin assay suggests that the amino grafting is the same for

20   both MCM-41-NH$_2$.

21   **3.3 Z- potential analyses.** More information were obtained through the Z- potential analyses,

22   measuring the surface charge of MCM-41 before and after the amino grafting. As expected, a

23   negative charge of -38 mV, typical of silica,[2] was found for MCM-41, that increased after the

1   functionalization. In particular, Z-potential values ranging from +30 to −44 mV, changing the pH

2   values (from 2 to 12), were obtained (**Figure 3),** confirming the amino grafting. It is worth noting,

3   that the surface charge of the MCM-41-NH$_2$ resulted positive, in the pH range from 2 to 9, due to

4   the amino groups protonation, and became negative when hard condition of pH were adopted, *i.e.*

5   up to pH 10, when the complete deprotonation of amino groups is expected, since the pK$_a$ of

6   primary amino groups was at about 9 units of pH.[42] Interestingly, the MCM-41-PRE Z-potential

7   values were almost zero, when was studied in neutral and slightly basic solutions, compared with

8   MCM-41-POST (**Figure 3**), under the same experimental conditions. These results could indicate

9   the amino groups presence especially inside the channels, when MCM-41-PRE were considered.

10   Indeed, the functionalization during the synthesis (MCM-41-PRE) was expected to be randomly

11   distributed, respect to the introduction POST synthesis (MCM-41-POST), in which the MCM-41

12   surface was largely available.

13   After these assessments related to the main properties of the synthetized MCM-41-NH$_2$, the DB

14   adsorption onto MCM-41-NH$_2$ was carried out, searching the best condition of work for an

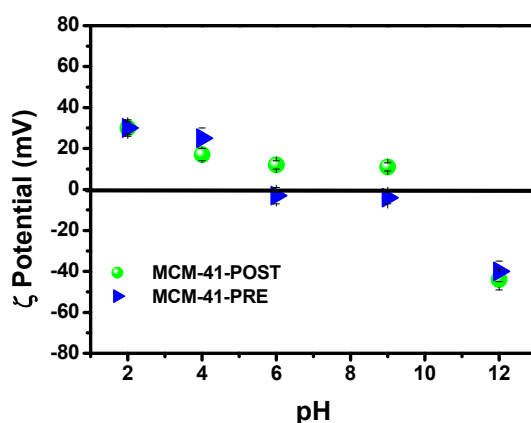15   efficient anionic dye removal from water.

Figure 3: Z-potential values of MCM-41-POST and PRE at several pH values ranging from 2 to 12.

16

1   **3.4 Overview about the adsorption test.** As initial phase, the DB adsorption onto MCM-41

2   without the functionalization was evaluated. The experiments were performed at 5.0×10^{-5} M DB

3   dye initial concentration, fixing the amount of the adsorbent material at 12 mg (into 2 mL of

4   aqueous dye solution), stirring the system for 24h, with a preliminary sonication of samples needed

5   to disperse particles. The results, observed and evaluated via UV-Visible absorption spectroscopy

6   (data not shown), indicated the absence of any adsorption onto MCM-41, under our experimental

7   conditions, due to the arising of electrostatic repulsion between the negative charges of dye and

8   MCM-41surface (Z-Potential: -38 mV). Indeed, DB has different functional groups (**Scheme 1**):

9   the sulfonate moieties, that occurred deprotonated in the pH range 2-12;[11] tertiary amino groups,

10   having a pK_a value at around pH 4; and secondary amino groups with a deprotonation that started

11   around pH 9.[11] The same experiment was thus performed decreasing the pH of the DB solution.

12   In that condition, MCM-41 acquired a positive charge and a Z-Potential value of +4 mV was

13   measured at pH 2. Notwithstanding the MCM-41 positively charged presence, the adsorption of

14   DB did not occur, indicating that naked MCM-41 were not suitable for the DB removal, probably

15   because the particle surface positive charge is not enough intense for a strong interaction. However,

16   it cannot be excluded that the adsorption process involves also non-electrostatic interactions.

17   Accordingly, the attention was focused on MCM-41-NH$_2$, characterized by a Z-potential more

18   positive than MCM-41. **Figure 4** reports the extraordinary results related to the DB adsorption

19   (5.0×10^{-5} M, 2 mL) by using 12 mg of MCM-41-NH$_2$, as adsorbent The camera pictures of the

20   dye solution, before and after the adsorption process, are reported and clearly indicated the

21   obtained results: clean water with a complete color bleaching was observed after few minutes

22   along with DB molecules entrapped in MCM-41-NH$_2$. Indeed, the brilliant blue color acquired by

23   the adsorbent after the DB adsorption better emphasizes the process, showing a uniform

1   macroscopic distribution of dyes molecules inside the active sites of the adsorbent. In detail,

2   **Figure S2A** shows step by step how the process occurred. In that case a large amount of colored

3   water was used to highlight the efficiency of the process and to show as the large amount of DB

4   and MCM-41-NH$_2$ induced the spontaneous separation of MCM-41-NH$_2$/DB from clean water

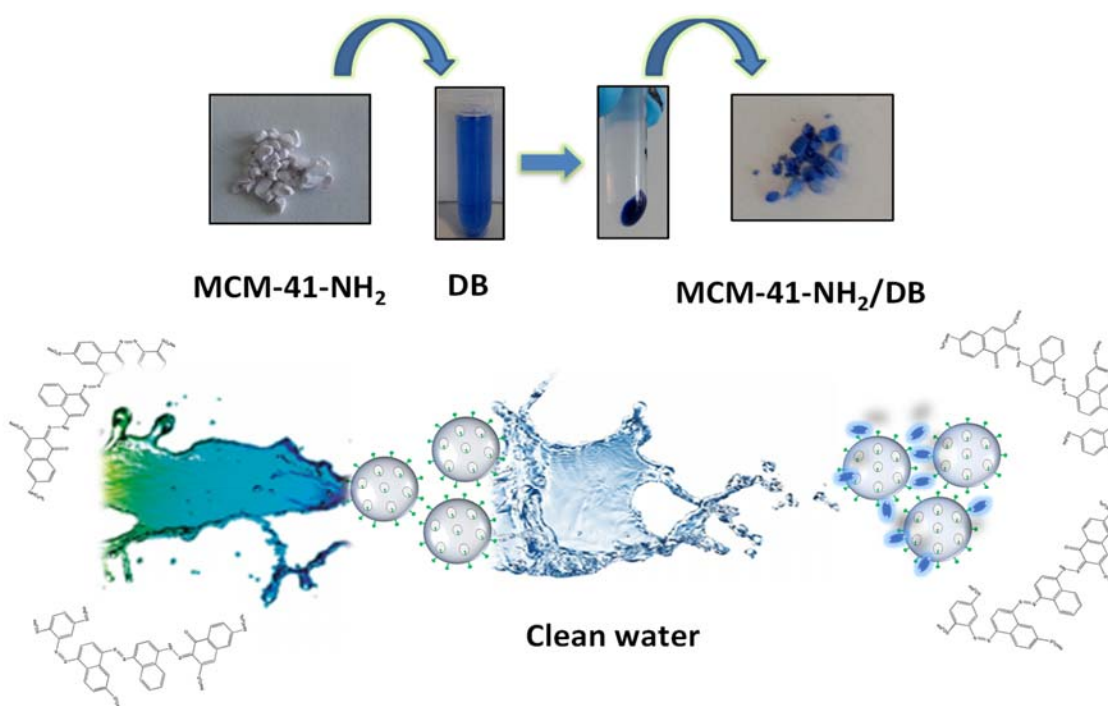5   making the process suitable for large scale applications.

Figure 4: Camera pictures of the MCM-41-NH$_2$ before and after the adsorption of DB (MCM-41-NH$_2$/DB) with the resulting solutions. Clean water was obtained after few minutes of contact time between the adsorbent (12 mg) and the DB solution.

6

7   Accordingly, by monitoring the main absorption band of DB at 600 nm, the DB complete

8   removal from water was observed within 5 minutes (**Figure 5A**). This typical DB absorption band

9   is a $\pi \rightarrow \pi^*$ transition, predominates the spectrum and is diagnostic for following the adsorption

10   process. In particular, this spectroscopic signal arises from the characteristic DB chromospheres

11   and from the interaction between azo functionality (–N=N–) and attached aromatic moieties.[11]

1   In agreement with in literature [11], lack of wavelength shifts in the DB absorption spectra, along

2   with slight changes in band intensity, were observed during this work, by changing the pH values

3   of solutions containing the dye in the range of pH 2-12 (**Figure S2B**); only at pH 2 the intensity

4   of the absorption band slightly decreased. The finding confirms the $\pi \rightarrow \pi^*$ nature of that band and

5   it could be attributed to the protonation of the central secondary amino group that induces the

6   disruption of hydrogen bonds planarizing the molecule.[11] Increasing the amount of the

7   adsorbent, the adsorption efficiency increased. More specifically, for MCM-41-PRE only 2.0 mg

8   were enough to rapidly adsorb (5 minutes) the dye from water, and the efficiency was as whole

9   reduced when 0.4 mg of the adsorbent were used (**Figure S3**). As for MCM-41-POST, a reduced

10   affinity was evident and, by using 2.0 mg of the adsorbent, 15 minutes were necessary to

11   completely remove the dye, with an important decrease in efficiency when 0.4 mg of the particles

12   were adopted (**Figure S4**). These results clearly evidenced the importance of amino groups

13   presence. As already mentioned, at neutral pH tertiary amino groups onto MCM-41-NH$_2$ are

14   protonated, suggesting a key role for electrostatic interactions during the DB adsorption process.

15   This finding was confirmed observing the SEM image shown in **Figure 5B.** As a whole, the DB

16   adsorption induced the MCM-41-NH$_2$ aggregation indicating the surface charge reduction of

17   MCM-41-NH$_2$/DB, due to the DB shielding of positively charged amino groups. Hence, after the

18   DB adsorption on MCM-41-NH$_2$, the Z-potential values decreased from $+12\pm2$ mV to 7 ± 1 mV for

19   MCM-41-POST and from 0 ± 3 mV to -9 ± 3 mV for MCM-41-POST, respectively. Overall, two

20   factors contributed to these results: i) the neutralization of charged amino groups by $-SO_3^-$ moieties

21   on the DB chemical structure and ii) the presence of free negative charges on DB that contributed

22   to the MCM-41-NH$_2$ global charge decrease.

1   Furthermore, for better highlighting the adsorption of DB inside the channels, the solid state

2   visible spectrum of MCM-NH$_2$/DB was collected observing the DB characteristic band (inset in

3   **Figure 5B**) already observed in **Figure 5A**. In order to give a deepest detailed investigation about

4   the mesostructured array after the DB molecules adsorption, SAXS analyses on MCM-41-NH$_2$/DB

5   were also performed (**Figure S5**, see blue and green patterns). The experiments suggested that the

6   interaction between DB and MCM-41-NH$_2$ did not affected the ordered structure, since the typical

7   diffraction peak of empty MCM-41-NH$_2$ was clearly evident. N$_2$ sorption isotherms were then
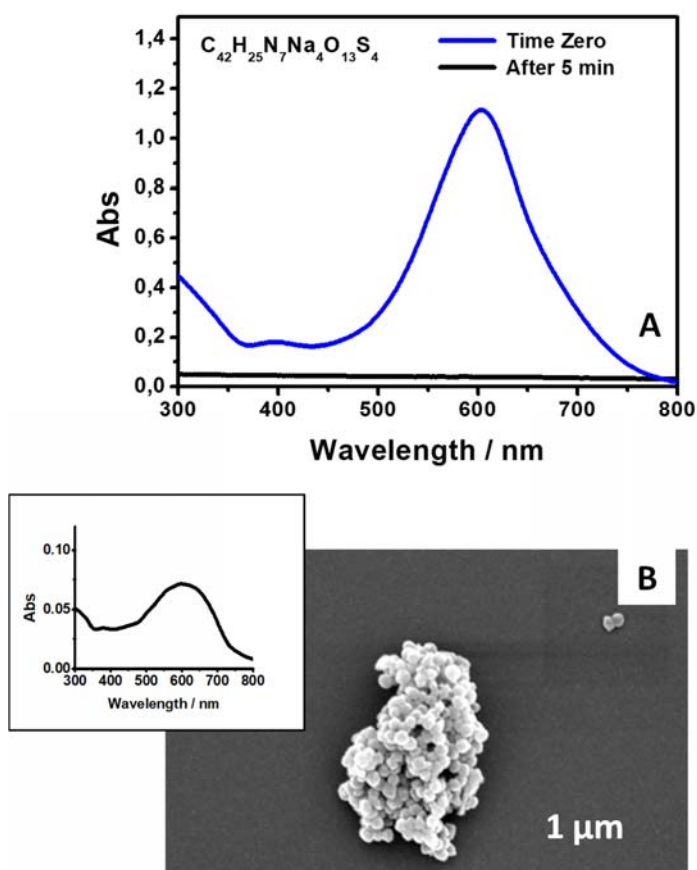

Figure 5: Comparison between the Visible absorption spectra obtained from DB aqueous solutions containing 5.0×10^{-5}M of DB (blue line) in absence of MCM-41-NH$_2$ and after 5 minutes adopted as contact time in presence of 12.0 mg/2mL of MCM-NH$_2$ **(A)**; SEM microphotograph of MCM-41-NH$_2$ after the adsorption of DB. In the inset of the same figure, the solid-state spectrum of DB is reported **(B)**.

8   acquired to investigate as the DB molecules occupied the pore volume of mesoporous structure.

1   Typical curves, already discussed for empty MCM-41-NH$_2$, (**Figure S6A**), were observed for

2   MCM-41-NH$_2$ in presence of DB. This finding indicated that the mesoporous structure was

3   retained also in presence of adsorbed DB molecules. At the same time, in the *p*/*p*$_0$ range (between

4   0.1 and 0.9), the adsorbed N$_2$ volume decreased, suggesting the presence of dye molecules

5   hindering the N$_2$ adsorption. In agreement, the pore volume decreased from 0.031 to 0.021 cm^3/g

6   for MCM-41-POST and to 0.27 cm^3/g for MCM-41-PRE (**Figure S6B**), respectively. Further, the

7   micropore widths were reduced from 3.5 nm to 2.8 nm for MCM-41-POST and to 2.7 nm for

8   MCM-41-PRE. These phenomena reflected the occupation the mesoporous structure by dye

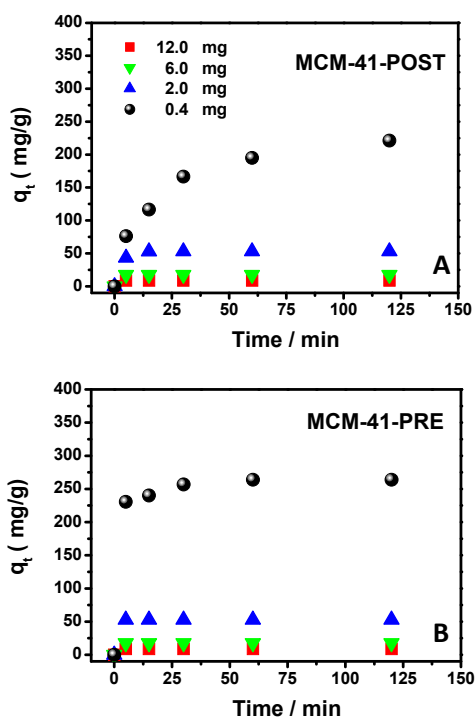9   molecules filling the MCM-41-NH$_2$ channels.[43]

Figure 6. Effect of MCM-41-POST (**A**) and PRE (**B**) amount (in mg/2mL of dye solution) on the adsorption capacity, q$_t$ (mg×g^{-1}), at time *t*, of DB removal from neutral aqueous solutions at 5.0×10^{-5}M concentration.

10

1   **3.5 Effect of adsorbent dosage and dye concentration.** The influences of the amount of MCM-

2   41-POST and PRE on DB adsorption was carefully evaluated calculating the q_t values using

3   **Equation 2** (**Figures 6A and B**). The dye solutions were monitored until the complete dye uptake,

4   however in **Figures 6** only the behavior of the first 150 minutes is reported. The results indicated

5   that at constant DB concentration (5.0×10^{-5} M), by increasing the adsorbent amount of MCM-41-

6   POST and PRE from 0.4 to 12.0 mg in 2 mL of dye aqueous solution, the adsorption of DB

7   molecules increased, but the adsorption capacity decreased. Interestingly, according to Anbia *et*

8   *al.*,[2] the increase in adsorption could be attributed to the surface area increasing and to the

9   availability of more free adsorption sites, while the decrease in adsorption capacity could be better

10   explained considering that some of the adsorption sites remained unsaturated during the adsorption

11   process.[2,6,11] Additionally, the aggregation of MCM-41-NH$_2$, observed when large material

12   amounts were used, under our experimental conditions, could be responsible of a reduced

13   adsorption capacity.[19,44]

14   These findings were in excellent agreement with those obtained decreasing the DB

15   concentration, as reported in **Figures 7**. In order to appreciate variations, the experiments were

16   performed using the smallest amount of the adsorbent material (0.4 mg/2 mL), studying the

17   behavior of two DB concentrations: 1.0×10^{-5}M and 5.0×10^{-5}M. **Figures 7A** and **B** show that, for

18   both MCM-41-POST and PRE, the relative maximum adsorption were obtained quickly, after few

19   minutes, when a small amount of dye was employed (see the first point in which the plateau region

20   was observed). Not surprisingly, by reducing the ratio dye/adsorbent materials, more adsorption

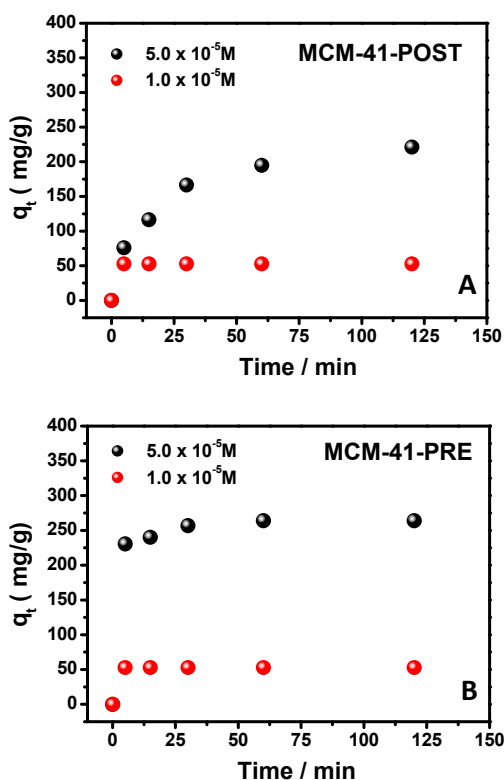21   sites were available.[6,11]

22

23

Figure 7: Effect dye concentration on the adsorption capacity, q_t (mg×g^{-1})at time t of DB removal from neutral aqueous solutions onto MCM-41-PRE (**A**) and POST (**B**). Measurements were performed adopting 0.4 mg/2mL of MCM-41-NH$_2$.

1   If the efficiency in the DB removal increased diluting the solution, the adsorption capacity

2   increased with more concentrated dye solutions (*i.e.* initial DB concentration of 5.0×10^{-5}M) and

3   such a behavior can be better explained by the higher concentration gradient at the MCM-41-

4   NH$_2$/solvent interface.[45] Indeed, by using a higher DB concentration, after the first 5 minutes, a

5   higher relative uptake was observed, in comparison with the results obtained for the diluted DB

6   solution. Overall, these results showed the high adsorption capacities of the presented adsorbents

7   with q$_{max}$ values of about 250 mg/g. Indeed, by using 0.4 mg of adsorbent and a DB solution

8   5.0×10^{-5}M the saturation of active sites tends to level off restituting the q$_{max}$. In the case of MCM-

9   41-PRE, due to the observed DB very fast removal, the adsorption capacity can be increased to

10   300 mg/g. Interestingly, the dynamics of the adsorption process can be better understood through

1   the kinetic analysis evaluation. **Equations 3** and **4** were used to find the best model able to fit the

2   experimental data and, as an example, the results related to MCM-41-POST are presented (results

3   reported in **Figures S7** and **S8** can be qualitatively applied for both MCM-41-NH$_2$). As shown in

4   **Figures S7 and S8**, the adsorption of DB dye molecules on MCM-41-POST and PRE followed a

5   pseudo-second-order kinetics, with an excellent regression coefficients (and R^2 ~ 1), excluding the

6   pseudo-first-order mechanism, whose calculated regression coefficients (*data not shown*) were

7   less than 0.99 (R^2<<0.99).[6,11] These results clearly confirmed the role of both the adsorbent and

8   dye amounts for obtaining an efficient adsorption process. More details about the nature of

9   interaction between DB and MCM-41-NH$_2$ were searched by changing the pH values of DB

10   solutions. Indeed, the pH of dye solution should affect both the surface charge of the adsorbent

11   and the degree of ionization of dye.[11]

12   **3.6 Effect of pH.** For studying the pH effect on the MCM-41-POST and PRE adsorption

13   capacity, dye solutions having pH values ranging from 2 to 12 were adopted. After the addition of

14   the adsorbent only slight changes on the measured pH values were detected during the adsorption

15   process. As reported in **Figure 8A**, the adsorption capacity, q$_t$, of MCM-41-POST, calculated for

16   each pH values, increased by decreasing the pH and the maximum adsorption capacity was

17   observed at pH 2. It is worth to mention that for each q$_t$ value, the DB adsorption amount was

18   calculated considering, as initial time, the DB absorption spectrum at each studied pH value at the

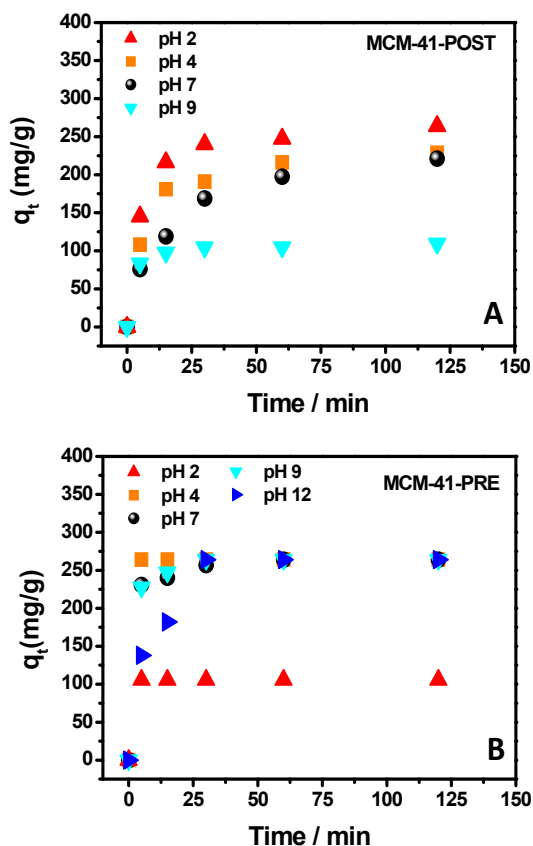19   beginning of the experiment (**Figure S2B**). As expected, at lowest pH value, the surface of MCM-

Figure 8: Effect of pH on the adsorption capacity q_t (mg×g^{-1}) at time t of DB from aqueous solutions (pH 2-12) onto MCM-41-POST (**A**) and from aqueous solutions (pH 2-9) onto MCM-41-PRE (**B**). Measurements were performed adopting 0.4 mg of mesoporous material for 2 mL of DB having a concentration of 5.0×10$^-$

1   41-POST resulted positively charged via the protonation process (see **Figure 3**), increasing the

2   electrostatic attractions between negatively charged dye and MCM-41-POST surface.[11,44]

3   On the other hand, at higher pH values, *i.e.* 9, the number of positively charged sites lowered

4   (primary amino groups pK$_a$ is 9), reducing the affinity between MCM-41-POST and the anionic

5   dyes molecules.[45] Indeed, as can be seen from **Figure 3**, a Z-potential near zero was observed

6   under this experimental condition.

7

8

1   Further increasing the pH to 12, the very high negative charge of the adsorbent (Z-potential value

2   of about -40 mV, **Figure 3**) unfavored the adsorption process and the DB adsorption did not occur

3   at all. Surprisingly, when MCM-41-PRE were studied (**Figure 8B**), the adsorption capacity

4   appeared to be the same in the range of pH from 6 to 9, and it was improved when pH 4 was

5   adopted as condition of work. On the other hand, the further decrease or increase of the pH (pH 2

6   or 12) reduced the affinity towards the adsorbent (**Figure 8B**). These findings can be once more

7   attributed to the electrostatic interaction between MCM-41-PRE and DB. Looking at the chemical

8   structure of the used dye (**Scheme 1**), at pH 2, the DB amino groups were protonated and, since

9   also MCM-41-PRE amino groups were positively charged (Z-potential=+30 mV at pH=2, **Figure**

10   **3**), MCM-41-PRE and DB molecules tended to repel. A similar scenario was already observed and

11   well described by Rizzi *et al.*[11] when DB was studied in presence of a Polyamidoamine-Based

12   Hydrogel as adsorbent.[11] This effect appeared only in this condition and with this material,

13   because the MCM-41-PRE amino grafting, carried out during the synthesis, distribute amino

14   groups also inside the pore channels. Therefore, the dye has to diffuse inside the channels, overall

15   slowing down the adsorption process, and establishing stronger interactions than those observed

16   for MCM-41-POST. This suggested that, when MCM-41-POST was used, weaker and superficial

17   interactions should be considered, favoring and improving the adsorption at pH 2. Whereas, the

18   slight less efficient adsorption at pH 12, where the amino groups were not protonated, suggested

19   that probably, between DB molecules and MCM-41-PRE, were present also other types of

20   interactions, as, for example, hydrogen bonds. This hypothesis explains the different behavior

21   observed at pH 9 if MCM-41-POST and PRE are compared. At pH. 9, the number of positively

22   charged sites was lowered (primary amino groups pK_a is 9), and a reduced affinity between MCM-

23   41-PRE and the anionic dyes molecules should be expected, as observed for MCM-41-POST.

1   Indeed, as can be seen from **Figure 3**, a Z-potential near zero was measured under this

2   experimental condition. Surprisingly, the results obtained at pH 9, restituting high q_t values,

3   indicated the presence of interaction, between DB and the adsorbent, different form electrostatic

4   one. Deeper interactions between MCM-41-PRE and DB molecules were thus supposed under

5   these experimental conditions of work. So, the presented results indicated as the maximum

6   adsorption capacity of the adsorbents can be improved changing the pH of the dye solutions.

7

8   **3.7 Effect of the phosphate anions on the adsorption process**. In order to better investigate the

9   role of electrostatic interactions, some experiments using a phosphate buffer solution (PBS) at pH

10   7, varying the electrolyte concentration, were performed.[46] PBS was chosen for maintaining

11   constant the solution pH value at 7, having already observed the great pH influence on the

12   adsorption process, but the salt concentration was changed in order to modify the solution ionic

13   strength. The DB concentration and the amount of MCM-41-NH$_2$ were fixed at 5.0×10^{-5} M and

14   0.4 mg/2 mL, respectively. In excellent agreement with the key role of electrostatic forces in the

15   adsorption process, variations were observed only when MCM-41-POST were studied (**Figure 9**).

16   Conversely, for MCM-41-PRE, no significant changes in the dye removal efficiency from water

17   was observed. This could be due or (i) to a so high performance of this mesoporous material, that

18   any solution modification is irrelevant, or (ii) to the involvement of interactions different from the

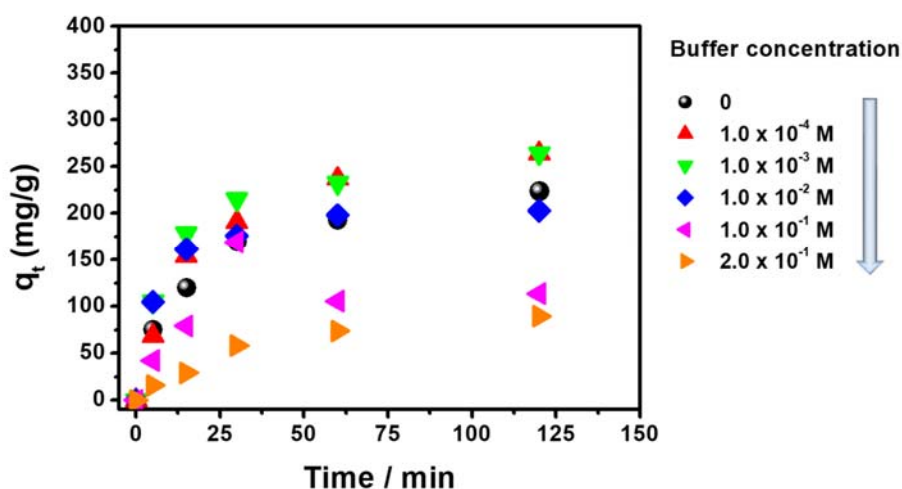19   electrostatic ones, as already supposed, investigating the pH 12 solutions.

Figure 9: Effect of PBS at different concentrations on the adsorption capacity, q_t (mg×g^{-1}) at time t, of DB from aqueous solutions onto MCM-41-POST. Measurements were performed adopting 0.4 mg of mesoporous material for 2 mL of DB solution at $5.0×10^{-5}$M.

1

2   In **Figure 9**, the results related to the use of MCM-41-POST are shown. The calculated q_t values

3   display that, using very high concentrations of phosphate ($1.0×10^{-1}$M and $2.0×10^{-1}$M), the

4   adsorption process was slowed down, due to the screen effect of the opposite charges both in the

5   adsorbents (PO_4^{3-} ions shield protonated amino group) and the dye molecules (monovalent cations

6   shield anionic moieties).[47] As a result, the attractive Coulombic potential between the adsorbate

7   molecules and the positively charged adsorbent material was screened, indicating also a

8   preferential interaction between the phosphate ions and the adsorbent active sites. Indeed, the salts

9   are small molecules and thus, was expected that they were able to efficiently compete with DB

10   during the adsorption process.[30] Interestingly, reducing PBS concentration, in the same

11   experimental conditions, the DB adsorption rate increased. More specifically, when the buffer

12   concentration was settled at $1.0×10^{-4}$ M and $1.0×10^{-3}$ M, the adsorption was very fast and was

13   accomplished in few hours, *i.e.* 2h against the 24h in absence of salt (**Figure 9**). These findings

14   suggested that the adsorption process is the result of a balance between attractive and repulsive

1   Coulombic forces. As already mentioned, DB has positively charged moieties (**Scheme 1**),

2   unfavorable to the attraction between its negatively charged sulfate groups and positive amino

3   groups on MCM-41-POST. Small amount of salt, shielding the repulsive forces, improving as a

4   whole the adsorption process.[27] In conclusion, all the experimental results suggested a different

5   way of interaction between dye molecules and MCM-41-PRE or MCM-41-POST. In particular,

6   using MCM-41-PRE, the adsorption of DB molecules was very fast and efficient, due to the

7   presence of both electrostatic interaction and H-bonds, able to block the dye also inside the

8   mesostructure of the adsorbent material, besides onto the material surface. While, employing

9   MCM-41-POST, since amino groups were mainly present on the material surface, only superficial

10   electrostatic interaction could block the dye on the adsorbent.

11   **3.8 Desorption experiments.** Thanks to the previous experimental results, in order to verify the

12   recycle of both adsorbent and adsorbate, some desorption experiments were carried out by

13   exploiting the solution pH influence. In detail, after the adsorption of DB molecules from a solution

14   at concentration of 5.0×10^{-5}M, DB/MCM-41-POST and DB/MCM-41-PRE (6 mg/2mL) were

15   recovered by centrifugation and put in solutions at different pH values, from 9 to 12.

16   Although, MCM-41-PRE occurred as the materials with the highest efficiency in the DB

17   removal from wastewater, thanks to the presence of stronger interaction, just these last ones

18   prevented the release of dye molecules from the mesoporous structure. **Figure S9** shows the

19   obtained results when a solution at pH 12 was adopted to desorb the dye. Owing to the presence

20   of strong interactions between DB and the adsorbent, the release was very low, obtaining the

21   maximum amount after 60 minutes of contact time; incrementing the contact time, in agreement

22   with the results obtained studying the adsorption at pH 12, the DB molecules were again adsorbed.

23   Interestingly, if MCM-41-POST were studied (**Figure 10A**), the dye release occurred rapidly with

1   a complete DB desorption from the mesoporous materials. Moreover, five cycles of

2   adsorption/desorption of DB on/from MCM-41-POST were achieved with very high efficiencies.

3   On this ground, the obtained q_{max} values of 250mg/g for each adsorption cycle can be potentially

4   increased, performing consecutive cycles of DB adsorption/desorption, by using the same

5   adsorbent.

6   In detail, after the first cycle of desorption, MCM-41-POST were previously neutralized in water

7   medium until pH 7. The Z-potential measure showed that the MCM-41-POST charge changed

8   from +10 mV before the adsorption, to -44 mV at pH 12 and to +5 mV after the neutralization in

9   water medium. Five cycles were performed without any change in the DB removal/recovery

10   efficiency (**Figure 10A**). However, although after the first cycle of desorption the properties of the

11   MCM-41-POST and the morphology were retained, unfortunately after 5 cycles of

12   adsorption/desorption, the mesoporous ordered array was disrupted, likely due to the strong basic

13   medium conditions. After the first cycle, SEM and N_2 adsorption experiments showed the absence

14   of significant changes in the MCM-41-POST morphology and properties (*data not shown*). A pore

15   width of 3.1 nm was measured, analogous to the incremental pore volume in empty MCM-41-

16   POST, confirming the complete release of the dye. In **Figure S5,** as example, the SAXS profile is

17   reported to evidence the absence of variation, induced by strong basic conditions, after the first

18   cycle of DB adsorption/desorption. The subsequent neutralizing process did not alter the SAXS

19   profile (**Figure S5**). Conversely, **Figure 10B** shows as the MCM-41-NH_2 typical diffraction peak,

20   arisen from SAXS experiments, disappeared after 5 cycles (by using alkaline water to desorb the

21   dye), indicating a disordered arrangement of pores. However, the particles appeared with their

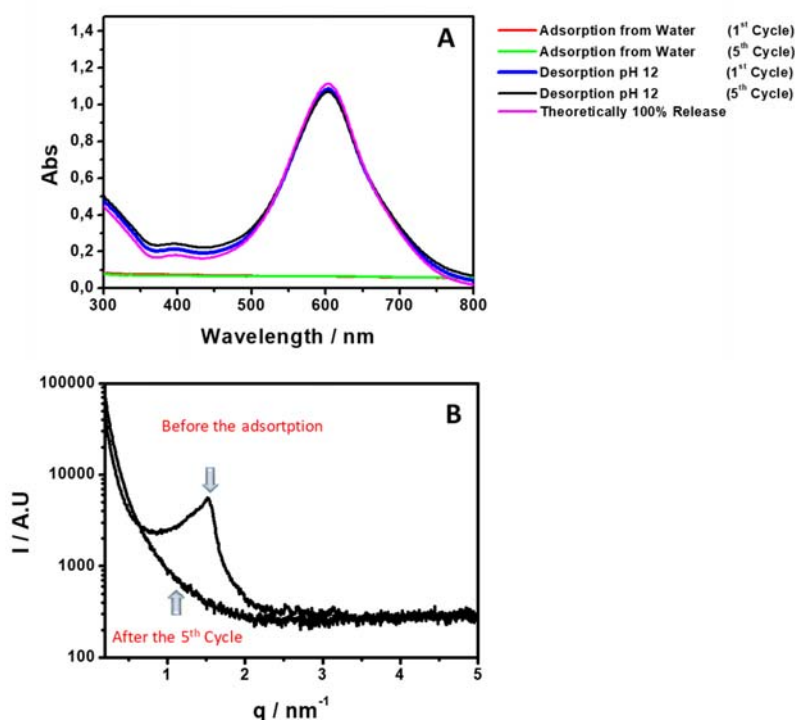22   typical morphology, retaining both the shape and size (**Figures S10**).

Figure 10: Comparison between the UV-Vis absorption spectra obtained from DB aqueous solutions before and after the adsorption on MCM-41-POST both after 1 cycle and 5 cycles of adsorption and desorption at pH 12 (**A**).SAXS patterns of MCM-41-POST before and after 5 cycles of adsorption/desorption of DB (**B**).The diffraction peak in the figure disappeared since the use of alkaline conditions of work used to desorb DB from the adsorbent after 5 cycles.

1

2   The **Scheme 2** depicts the possible mechanism of DB adsorption/desorption when MCM-41-

3   POST were used as adsorbent. The role of electrostatic interaction along with the H-bond are

4   evidenced, showing as the presence of the negatively charged adsorbent determined the dye release

5   due to the involvement of repulsive forces.

6   It is worth to mention that the DB chemical and physical properties were not affected after the

7   adsorption/desorption processes. Indeed, the spectrum after the release occurred to be the same in

8   comparison with that recorded before the adsorption process at pH 12, confirming such hypothesis.

9   Moreover, measurements related to the lifetime of excited dye $^1DB^*$ were also performed, ensuring

10   the absence of degradation processes during the adsorption process. In detail, the same

1   biexponential decay was observed in our condition, with lifetimes that resulted to be t_1=10.60 ns

2   (6.08 %) and t_2=3.70 ns (93.92 %) before the DB adsorption, and t_1=11.80 ns (1.4 %) and t_2=3.70

3   ns (98.6 %) after the DB desorption at pH 12.
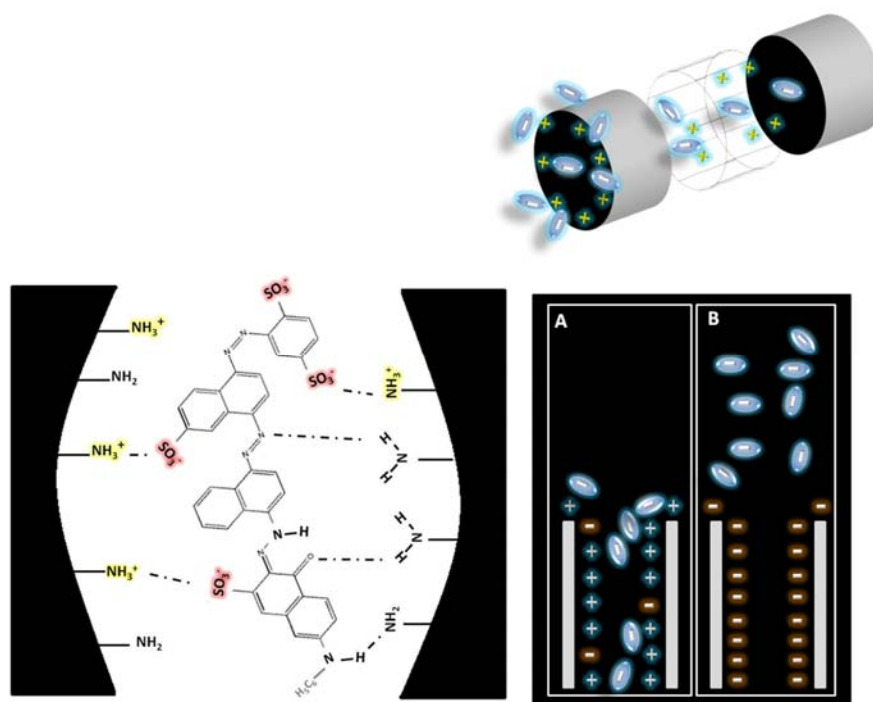
Scheme 2: Graphic design of pore channels in the presence of dye: DB absorbing molecules in neutral or acid medium on MCM-41-POST or PRE **(A)** and DB molecules during the release from MCM-41-POST **(B)**. The picture describes also the nature of interaction involved during the adsorption process.

4

5   **3.9 Isotherms of adsorption.** The adsorption isotherms reported as **Equations 5-7** are important

6   key features for describing the adsorption mechanism between DB and the adsorbent surface [11].

7   For this purpose, experiments were performed by adopting three DB solutions having different

8   concentrations (5.0×10^{-5}M, 2.5×10^{-5}M and 1.0×10^{-5}M) in presence of 0.4 mg of adsorbent.

9   **Figures S11-S12** reported the results by adopting Langmuir, Freundlich and Temkin isotherms

10 both for MCM-41-PRE and POST. By looking the R^2 values, both Freundlich and Temkin

11 isotherms well fitted the experimental data for MCM-41-POST and PRE, suggesting that the

12 adsorption occurred onto heterogeneous surfaces. [11] Further, the Temkin model indicated that

1   the heat of adsorption decreased during the adsorption process. The related isotherm constants

2   arisen from the employed models are reported in **Tables S1** and **S2**. Interestingly, the *n* values,

3   indicated in the Freundlich equation (**Table S1** and **S2**), represents the adsorption strength, and

4   values ranged from 1 to 10 indicates, as in this case, that the adsorption process was favored.

5

6   **4. CONCLUSIONS.**

7   The synergic use of several experimental techniques enabled a careful investigation of the DB,

8   a negatively charged dye, adsorption on amino grafted MCM-41-NH_2. For the first time, during

9   this work the very high removal of DB (q_{max} of around 300 mg/g) by using amino grafted MCM-

10   41 is thus presented. Moreover, both the change of the dye solution pH-values and the increase of

11   the ionic strength can improve the performance of the adsorbents reducing the contact time needed

12   to adsorb DB. With respect the previous literature [27-32], in which q_{max} values in the range 10-

13   280 mg/g were obtained, in the present paper the reuse of the adsorbent is proposed increasing the

14   removed DB amount by using the same adsorbent; at least the environmental impact and the

15   associated costs are lowered considering also the DB reuse. Indeed, with respect other similar

16   studies [29, 32], the use of organic solvents and/or hard condition of work, as calcination, to desorb

17   DB, are avoided by using only alkaline water. In this way the found q_{max} values could be potentially

18   increased considering the possibility to perform adsorption/desorption cycles.

19   In detail, two different approaches were used to introduce amino groups on MCM-41: i) during

20   the synthesis (MCM-41-PRE) and ii) after the synthesis, meaning after the calcinations (MCM-

21   41-POST). The amino grafting inside and outside the pore was obtained, respectively. The key

22   role of amino groups in affecting the adsorption of DB from wastewater was evidenced, by

23   comparing the results obtained during the use of MCM-41 and by information inferred during the

1   Z-potential analyses. The presence of electrostatic interactions was suggested and confirmed

2   through experiments performed by changing the pH values in the range 2-12, and the ionic strength

3   of the DB solutions using the phosphate buffer as additional electrolyte. A different behavior was

4   observed for MCM-41-POST and PRE. Indeed, although both materials are affected by very acidic

5   or basic conditions, the former exhibits a stronger dependence of qt on the pH value: the adsorption

6   capacity increases at acidic pH and decreases at basic condition. While, MCM-41-PRE results less

7   dependent on the pH changes, suggesting the involvement of other forces together with the

8   electrostatic ones, during the adsorption process. Accordingly, the presence of electrolytes

9   influenced only the adsorption capacity of MCM-41-POST, retarding the adsorption if present in

10   high concentrations. Further, the study was performed by changing both the amount of the

11   adsorbent and the dye, evaluating the process kinetics. The pseudo-second-order model resulted

12   the best fitting equation, depending both on the concentration of the DB and adsorbent. Indeed, by

13   decreasing the DB concentration and increasing the amount of the adsorbent the adsorption process

14   improved, on the other hand the use of more concentrated dye solutions in presence of small

15   amount of adsorbent increased the time necessary to adsorb completely the dye. The release of the

16   DB molecules was also obtained using MCM-41-POST, enabling in very short time the possibility

17   to recycle both the adsorbent and the anionic dye. In agreement with the lack of adsorption

18   observed at pH 12 when MCM-41-POST were used, the release of DB occurred under these

19   experimental conditions, emphasizing the main role of electrostatic interactions. On the other hand,

20   the absence of the release obtained for MCM-41-PRE suggested the presence of different forces

21   involved during the DB adsorption, as already supposed studying the pH effect of the DB solutions.

22   Novel horizons in the field of wastewater purification from toxic dyes by using low cost and

23   handily materials are presented during this work, with the possibility to perform very fast several

1 cycles of DB adsorption/desorption. Moreover, the DB reuse is also proposed, since the molecule

2 preserves its physical and chemical properties, as observed by looking the DB absorption spectrum

3 before and after the release, that occurred to be the same, and by studying the same [1]DB* lifetime

4 in the same conditions. Work is in progress about the possibility to perform experiments with

5 mixture of azo dyes searching the best conditions of work to treat real effluents.

6

13

14

15 **REFERENCES**

16 [1] Buthelezi, S.P.; Olaniran, A.O.; Pillay, B. Textile Dye Removal from Wastewater Effluents

17 Using Bioflocculants Produced by Indigenous Bacterial Isolates. *Molecules* **2012**, *17*,

18 14260-14274.

19 [2] Anbia, M.; Salehi, S. Removal of acid dyes from aqueous media by adsorption onto amino-

20 functionalized nanoporous silica SBA-3. *Dyes and Pigm.* **2012**, *94*, 1-9

21 [3] Robinson, T.; McMullan, G.; Marchant, R.; Nigam, P. Remediation of dyes in textile

22 effluent: a critical review on current treatment technologies with a proposed alternative.

23 *Bioresour. Techn.* **2001**, *77*, 247-255.

1   [4] Singh, K.P.; Mohan, D.; Sinha, S.; Tondon, G.S.; Gosh, D. Color Removal from

2   Wastewater Using Low-Cost Activated Carbon Derived from Agricultural Waste Material.

3   *Ind. Eng. Chem. Res.* **2003,** *42,* 1965-1976.

4   [5] Forgacs, E.; Cserháti, T.; Oros, G. Removal of synthetic dyes from wastewaters: a review.

5   *Environ. Int.* **2004**, *30*, 953-971

6   [6] Rizzi, V.; D'Agostino, F.; Fini, P.; Semeraro, P.; Cosma P. An interesting environmental

7   friendly cleanup: The excellent potential of olive pomace for disperse blue

8   adsorption/desorption from wastewater. *Dyes and Pigm.* **2017**, *140*, 480-490;

9   [7] Rizzi, V.; Longo, A.; Fini, P.; Semeraro, P.; Cosma,, P.; Franco E.; García, R.; Ferrándiz,

10   M.; Núñez, E.; Gabaldón, J.A.; Fortea, I.; Pérez, E.; Ferrándiz, M. Applicative Study (Part

11   I): The Excellent Conditions to Remove in Batch Direct Textile Dyes (Direct Red, Direct

12   Blue and Direct Yellow) from Aqueous Solutions by Adsorption Processes on Low-Cost

13   Chitosan Films under Different Conditions. *Adv. Chem. Eng. Sci.* **2014**, *4*, 454-469.

14   [8] Semeraro, P.; Fini, P.; D'Addabbo, M.; Rizzi, V.; Cosma, P. Removal from wastewater

15   and recycling of azo textile dyes by alginate-chitosan beads. *International Journal of*

16   *Environment, Agriculture and Biotechnology (IJEAB)* **2017**, *2(4)*, 1835-1850.

17   [9] Rizzi, V.; D'Agostino, F.; Gubitosa, J.; Fini, P.; Petrella, A.; Agostiano, A.; Semeraro, P.;

18   Cosma, P. An Alternative Use of Olive Pomace as a Wide-Ranging Bioremediation

19   Strategy to Adsorb and Recover Disperse Orange and Disperse Red Industrial Dyes from

20   Wastewater *Separations* **2017**, *4*, 29.

21   [10]   Rizzi, V.; Mongiovì, C.; Fini, P.; Petrella, P.; Semeraro, P.; Cosma, P. Operational

22   parameters affecting the removal and recycling of direct blue industrial dye from

1   wastewater using bleached oil mill waste as alternative adsorbent material. *International*

2   *Journal of Environment, Agriculture and Biotechnology (IJEAB)* **2017**, *2(4)*, 1560-1572.

3   [11]   Rizzi, V.; Fiorini, F.; Lamanna, G.; Gubitosa, J.; Prasetyanto, E.A.; Fini, P.; Fanelli,

4   F.; Nacci, A.; De Cola, L.; Cosma, P. Polyamidoamine-Based Hydrogel for Removal of

5   Blue and Red Dyes from Wastewater. *Adv. Sustainable Syst.* **2018**, 1700146

6   [12]   Rizzi, V.; Longo, A.; Placido, T.; Fini, P.; Gubitosa, J.; Sibillano,T.; Giannini, C.;

7   Semeraro, P.; Franco, E.; Ferrandiz, M.; Cosma, P. A comprehensive investigation of dye–

8   chitosan blended films for green chemistry applications. *J. Appl. Polym. Sci.* **2018**, *135(10)*,

9   45945

10   [13]   Semeraro, P.; Rizzi, V.; Fini, P.; Matera, S.; Cosma, P.; Franco, E.; García, R.;

11   Ferrandiz, M.; Núñez, E.; Gabaldón, J.A.; Fortea, I.; Pérez, E. Interaction between

12   industrial textile dyes and cyclodextrins. *Dyes and Pigm.* **2015**, *119*, 84–94.

13   [14]   Ekambaram, S.P.; Perumal, S.S.; Rajendran, D.; Samivel, D.; Khan, M.N. In

14   *Toxicity and Biodegradation Testing. Methods in Pharmacology and Toxicology*; Bidoia,

15   E., Montagnolli, R., Eds.; Humana Press, N.Y.; 2018, 241-267

16   [15]   Sivamani, S.; Leena, G.B. Removal of Dyes from Wastewater using Adsorption- A

17   Review *Intl. J. BioSciences and Technology* **2009**, *2(4)*, 47-51.

18   [16]   Seow, T.W.; Lim, C.K. Removal of Dye by Adsorption: A Review. *Int. J. Appl.*

19   *Eng. Res.* **2016**, *11(4)*, 2675-2679

20   [17]   Cestaria, A.R.; Vieira, E.F.S.; Vieira, G.S.; da Costa, L.P.; Tavares, A.M.G.; Loh,

21   W.; Airoldi, C. The removal of reactive dyes from aqueous solutions using chemically

22   modified mesoporous silica in the presence of anionic surfactant—The temperature

dependence and a thermodynamic multivariate analysis. *J. Hazard. Mat.* **2009**, *161*, 307–316

[18]   Nesic, A.R.; Kokunesoski, M.J.; Volkov-Husovic, T.D.; Velickovic, S.J. New method for quantification of dye sorption using SBA mesoporous silica as a target sorbent. *Environ. Monit. Assess.* **2016**, *188*, 160

[19]   Salahshoor, Z.; Shahbazi, A. Review of the use of mesoporous silicas for removing dye from textile wastewater. *Eur. J. Environ. Sci.* **2014**, *4(2)*, 116–130

[20]   Ho, K.Y.; McKay, G.; Yeung, K.L. Selective Adsorbents from Ordered Mesoporous Silica. *Langmuir* **2003,** *19,* 3019-3024

[21]   Huang, C.-H.; Chang, K.-P.; Ou, H.-D.; Chiang, Y.-C.; Wang, C.-F. Adsorption of cationic dyes onto mesoporous silica. *Micropor. Mesopor. Mat.* **2011**, *141*, 102–109

[22]   Wang, S.; Li, H. Structure directed reversible adsorption of organic dye on mesoporous silica in aqueous solution. *Micropor. Mesopor. Mat.* **2006**, *97*, 21–26

[23]   Zarezadeh-Mehrizi, M.; Badiei, A. Highly efficient removal of basic blue 41 with nanoporous silica, *Water Resources and Industry* **2014**, *5*, 49–57.

[24]   Kabakcı, S.B.; Aydemir, H. Pyrolysis of olive pomace and copyrolysis of olive pomace with refuse derived fuel. *Environ. Prog. Sustainable Energy* **2013**, *33*, 649-656.

[25]   Lu, H-T. Synthesis and Characterization of Amino-Functionalized Silica Nanoparticles *Colloid Journal* **2013**, *75(3)*, 311–318

[26]   Grisorio, R.; Piliego, C.; Striccoli, M.; Cosma, P.; Fini, P.; Gigli, G.; Mastrorilli, P.; Suranna, G.P.; Nobile, C.F. Influence of Keto Groups on the Optical, Electronic, and Electroluminescent Properties of Random Fluorenone-Containing Poly(fluorenylene-vinylene)s. *J. Phys. Chem. C* **2008**, *112(50)*, 20076-20087

1   [27]   Wang, Y.; Du, T.; Zhou, L.; Song, Y.; Che, S.; Korean, X.F. Removal of Acid Red

2   G dye from aqueous solutions by adsorption to MCM-41-layered double hydroxides

3   composite. *J. Chem. Eng.* **2018**, *35(3)*, 709.

4   [28]   Adlnasab, L.; Ezoddin, M.; Karimi, M.A.; Hatamikia, N. MCM-41@Cu–Fe–LDH

5   magnetic nanoparticles modified with cationic surfactant for removal of Alizarin Yellow

6   from water samples and its determination with HPLC. *Res Chem Intermed* **2018**, *44*, 3249.

7   [29]   Qin, P.; Yang, Y.; Zhang, X.; Niu, J.; Yang, H.; Tian, S.; Zhu, J.; Lu, M. Highly

8   Efficient, Rapid, and Simultaneous Removal of Cationic Dyes from Aqueous Solution

9   Using Monodispersed Mesoporous Silica Nanoparticles as the Adsorbent. Nanomaterials

10   2018, 8, 4.

11   [30]   Mirzaie, M.; Rashidi, A.; Tayebi, H.A.; Yazdanshenas, M. E. Optimized Removal

12   of Acid Blue 62 from Textile Waste Water by SBA-15/PAMAM Dendrimer Hybrid Using

13   Response Surface Methodology. *J Polym Environ* **2018**, *26*, 1831

14   [31]   Boukoussa, B.; Hakiki, A.; Moulai, S.; Chikh, K.; Kherroub, D. E.; Bouhadjar, L.;

15   Guedal, D.; Messaoudi, K.; Mokhtar, F.; Hamacha, R. Adsorption behaviors of cationic

16   and anionic dyes from aqueous solution on nanocomposite polypyrrole/SBA-15. *J Mater*

17   *Sci* **2018**, *53*, 7372.

18   [32]   Dong, Y.; Lu, B.; Zang, S.; Zhao, J.; Wang, X.; Cai, Q. Removal of methylene blue

19   from coloured effluents by adsorption onto SBA-15. *J Chem Technol Biotechnol* **2011**, *86*,

20   616.

21

[33]   Arami, M.; Limaee, N.Y.; Mahmoodi, N.M.; Tabrizi, N.M. Removal of dyes from colored textile wastewater by orange peel adsorbent: Equilibrium and kinetic studies. *J. Coll. Interf. Sci.* **2005**, *288(2)*, 371–376.

[34]   McKay, G.; Ho, Y.S. Pseudo-second order model for sorption processes. *Process. Biochem.* **1999**, *34*, 451–465.

[35]   Kachbouri, S.; Mnasri, N.; Elaloui, E.; Moussaoui, Y. Tuning particle morphology of mesoporous silica nanoparticles for adsorption of dyes from aqueous solution. *J. Saudi Chem. Soc.* **2017**, *22*, 405-415

[36]   Mohseni, M.; Gilani, K.; Mortazavi, S. A. Preparation and Characterization of Rifampin Loaded Mesoporous Silica Nanoparticles as a Potential System for Pulmonary Drug Delivery. *Iran J. Pharm. Res.* **2015**, *14(1)*, 27-34

[37]   Chung, T.H.; Wu, S.H.; Yao, M.; Lu, C.W.; Lin, Y.S.; Hung, Y.; Mou, C.Y.; Chen, Y.C.; Huang, D.M. The effect of surface charge on the uptake and biological function of mesoporous silica nanoparticles in 3T3-L1 cells and human mesenchymal stem cells. *Biomaterials* **2007**, *28*, 2959–2966

[38]   Suteewong, T.; Sai, H.; Lee, J.; Bradbury, M.; Hyeon, T.; Gruner, S.M.; Wiesner, U. Ordered mesoporous silica nanoparticles with and without embedded iron oxide nanoparticles: structure evolution during synthesis. *J. Mater. Chem.* **2010**, *20*, 7807–7814.

[39]   Zhang, T.; Xu, G.; Puckette, J.; Blum, F.D. Effect of Silica on the Structure of Cetyltrimethylammonium Bromide. *J. Phys. Chem. C* **2012**, *116* (21), 11626–11634.

[40]   Kailasam, K; Muller, K. Physico-chemical characterization of MCM-41 silica spheres made by the pseudomorphic route and grafted with octadecyl chains. *J. Chrom A*, **2008**, *1191*, 125–135

1   [41]   Badiei, A.; Mirahsani, A.; Shahbazi, A.; Younesi, H.; Alizadeh, M. Adsorptive

2   removal of toxic dye from aqueous solution and real industrial effluent by tris(2-

3   aminoethyl)amine functionalized nanoporous silica. *Environ. Prog. Sustainable Energy*

4   **2014**, *33*, 1242.

5   [42]   Zhuang, X.; Wan, Y.; Feng, C.; Shen, Y.; Zhao, D. Highly Efficient Adsorption of

6   Bulky Dye Molecules in Wastewater on Ordered Mesoporous Carbons. *Chem. Mater.*

7   **2009**, *21*, 706–716

8   [43]   Gerçel, O.; Ferdi Gerçel, H.; Savaş Koparal, A.; Öğütveren, U.B. Removal of

9   disperse dye from aqueous solution by novel adsorbent prepared from biomass plant

10   material. *J. Hazard. Mat.* **2008**, *160*, 668–674

11 [44]   Shirsath, S.R.; Patil, A.P.; Patil, R.; Naik, J.B.; Gogate P.R.; Sonawane, S.H.

12   Removal of Brilliant Green from wastewater using conventional and ultrasonically

13   prepared poly(acrylic acid) hydrogel loaded with kaolin clay: a comparative study.

14   *Ultrason. Sonochem.* **2013**, *20*, 914

15 [45]   Bharathi, K.S.; Ramesh, S.T. Removal of dyes using agricultural waste as low-cost

16   adsorbents: a review. *Appl. Water Sci.* **2013**, *3(4)*, 773–790

17

18 [46]   Mahmoodi, N.M.; Salehi, R.; Arami, M. Binary system dye removal from colored

19   textile wastewater using activated carbon: Kinetic and isotherm studies. *Desalination* **2011**,

20   *272(1–3)*, 187–195

21 [47]   Al-Degs, Y.S.; El-Barghouthi, M.I.; El-Sheikh, A.H.; Walker, G.M. Effect of

22   solution pH, ionic strength, and temperature on adsorption behavior of reactive dyes on

23   activated carbon. *Dyes and Pigm.* **2008**, *77*, 16-23

1

2

3